J Mater Sci (2013) 48:8539–8546
DOI 10.1007/s10853-013-7672-3

Microstructural evolution and superplastic behavior in friction stir processed Mg–Li–Al–Zn alloy

F. C. Liu · M. J. Tan · J. Liao · Z. Y. Ma · Q. Meng · K. Nakata

Received: 20 June 2013 / Accepted: 12 August 2013 / Published online: 29 August 2013

Abstract A Mg–Li–Al–Zn alloy was friction stir processed (FSP) under water, and the microstructures and superplastic behavior in the FSP alloy were investigated. The FSP Mg–Li–Al–Zn alloy consisted of a mixed microstructure with fine, equiaxed, and recrystallized α (hcp) and β (bcc) grains surrounded by high-angle grain boundaries, and the average grain size of the α and β grains was ~1.6 and ~6.8 μm, respectively. The fine α grains played a critical role in providing thermal stability for the β grains. The FSP Mg–Li–Al–Zn alloy exhibited low-temperature superplasticity with a ductility of 330 % at 100 °C and high strain rate superplasticity with ductility of ≥400 % at 225–300 °C. Microstructural examination and superplastic data analysis revealed that the dominant deformation mechanism for the FSPed Mg–Li–Al–Zn alloy is grain boundary sliding, which is controlled by the grain boundary diffusion in the β phase.

F. C. Liu (✉) · M. J. Tan (✉)
School of Mechanical and Aerospace Engineering, Nanyang Technological University, Singapore 639798, Singapore
e-mail: fchliu@alum.imr.ac.cn

M. J. Tan
e-mail: mmjtan@ntu.edu.sg

F. C. Liu · K. Nakata
JWRI, Osaka University, 11-1 Mihigaoka Ibaraki, Osaka 567-0047, Japan

J. Liao
Kurimoto Ltd, 2-8-45 Suminoe, Osaka 559-0021, Japan

Z. Y. Ma
Shenyang National Laboratory for Materials Science, Institute of Metal Research, Chinese Academy of Sciences, 72 Wenhua Road, Shenyang 110016, China

Q. Meng
Beijing Aeronautical Manufacturing Technology Research Institute, Beijing 100024, China

Introduction

Mg–Li-based alloys are expected to be extensively used in aerospace, automobile, and defense industries in the 21st century because of their ultra-low density, high strength/mass and elastic-modulus/mass ratios [1, 2]. According to the binary Mg–Li phase diagram [3], when the lithium content lies between ~5.7 and 11 mass %, the body-centered cubic (BCC)-structured β phase (Li solid solution) will co-exist with the hexagonal close-packed (HCP) structured α phase (Mg solid solution). The presence of a second phase is beneficial to superplasticity because grain growth is too rapid in single phase materials at temperatures where grain boundary sliding (GBS) occurs [4].

Superplasticity has attracted considerable scientific research because it presents significant challenges in the understanding of material flow and fracture, and also because it forms the underlying basis for the commercial superplastic forming industry in which complex shapes are formed from superplastic sheet metals [5, 6]. Either an increase in strain rate or a decrease in the temperature at which superplasticity appears is attractive for practical industrial production. This is because high strain rate superplasticity (HSRS), with strain rates $\geq 1 \times 10^{-2}$ s^{-1}, enables forming at a strain rate ten times faster than conventional superplastic forming [7] and also low-temperature superplasticity (LTSP) is beneficial to energy savings, grain stability, cavitation restriction, and surface solute loss prevention, thereby maintaining superior postforming properties [8].

Since grain refinement would lead to an increase in the strain rate or a decrease in the deformation temperature [9, 10], much effort has been made to refine the grains of Mg–Li-based alloys for achieving HSRS and/or LTSP [11–15]. Taleff et al. [11] have reduced the grain size of Mg–9Li alloy to 2.7 μm two decades ago through cold rolling and press-bonding the foils repeatedly up to a total reduction of 1200:1 at low temperatures and obtained an elongation-to-failure of 450 % at 100 °C and 5.6×10^{-4} s^{-1}. During the past decade, multi-pass equal channel angular extrusion [12, 13] and high ratio extrusion [14, 15] have been extensively used to refine the grains of dual-phase Mg–Li base alloys for the purpose of increasing the superplastic deformation rate or reducing the superplastic deformation temperature. However, it remains a challenge in achieving HSRS at low temperatures in Mg–Li-based alloys.

Friction stir processing (FSP), which was developed for microstructural modification based on the basic principles of friction stir welding [16], can be used to produce fine-grained materials with predominant high-angle grain boundaries (HAGBs) [17–20], which is critical to enhance superplasticity. Previous investigation showed that overlapping FSP passes could produce large-scaled fine-grained sheets and did not exert obvious effect on the grain size and superplasticity [21, 22]. Such bulk fine-grained materials are suitable to practical application. Although some investigations have been conducted to understand the effects of FSP on superplasticity of Al alloys and HCP-structured Mg alloys [17–23], to the best of the authors' knowledge, no attempt has been made to evaluate the effect of FSP on the microstructural evolution and superplasticity of dual-phase Mg–Li-based alloys.

Primary studies have suggested that materials with ultrafine grains could be prepared by means of active cooling during FSP [16–18]. Based on this consideration, FSP was conducted on a Mg–Li–Al–Zn alloy under water in this study. The objective is threefold: (i) to examine the microstructural evolution during FSP; (ii) to identify the possibility of achieving LTSP and HSRS in Mg–Li–Al–Zn alloy; and (iii) to elucidate the superplastic deformation mechanism of FSP Mg–Li–Al–Zn alloy.

Experimental

The as-received Mg–Li–Al–Zn ingot, with a composition of 9.93Li–3.06Al–1.49Zn (in wt%), was cut into 20-mm-thick plates initially, and then was cross-rolled to a thickness of 6 mm at room temperature with cross angle of 90° for each pass for the purpose of obtaining flat surfaces. A single-pass FSP was carried out on the rolled plate at a tool rotation rate of 400 rpm and a traverse speed of 50 mm min^{-1}. The tool was manufactured from M42 steel with a concave shoulder 16 mm in diameter and a threaded conical pin 5 mm in root diameter, 4 mm in tip diameter, and 3.8 mm in length. During FSP, the plate was completely submerged in water, and this novel FSP technique is called submerged FSP hereafter in the present paper. During the submerged FSP, flowing water was also used to quench the plate immediately behind the FSP tool in order to further inhibit the growth of the recrystallized grains.

To check the thermal stability of the fine grains introduced by FSP, small samples with dimensions of $6 \times 6 \times 10$ mm^3 were cut from the center of the stir zone (SZ), and were statically annealed for 1 h at selected temperatures from 100 to 300 °C and then followed by water quenching. To evaluate the superplastic capability of the FSP Mg–Li–Al–Zn alloy, dog-bone shaped tensile specimens (2.5 mm gage length, 1.4 mm gage width, and 1.0 mm gage thickness) were electrodischarge machined perpendicular to the FSP direction, with the gage length being centered in the SZ. These specimens were subsequently ground and polished to a final thickness of ~0.8 mm. All specimens were held at the selected temperature for 20 min to establish thermal equilibrium prior to the tensile test. Constant crosshead speed tensile tests were conducted using a Shimadzu 4830 tester. In order to investigate the microstructure evolution, the failed tensile sample deformed at 1×10^{-3} s^{-1} and 200 °C was subjected to microstructural examination on both the gage and grip region. The materials in the gage region experienced a combination of static annealing (holding at 200 °C for 20 min) and dynamic annealing (105 min during superplastic deformation), while the materials in the grip region merely experienced a static annealing at 200 °C for about 125 min.

Microstructural characterization was performed on the rolled, the FSP, the annealed, and the superplastically deformed samples by scanning electron microscopy (SEM). Before being subjected to SEM examination, these samples were mounted, mechanically polished, and then etched in a 2 vol% solution of HNO_3 and 98 vol% C_2H_5OH for about 1–2 min to reveal the microstructures. The rolled and FSP samples for electron backscatter diffraction (EBSD) investigations were prepared using an ion polisher (JEOL SM-09010). EBSD maps were obtained using a field emission scanning electron microscope (JEOL JSM-7000F), operated at 15 kV and scanning step of 100 nm.

Results

Microstructural characteristics

Figure 1a shows that the rolled Mg–Li–Al–Zn alloy was composed of light gray particles and dark gray matrix. The

Mg element distribution map produced by energy dispersive spectrometer showed that the light gray particles contained a higher concentration of Mg than the dark gray matrix (Figs. 1b, c). This is in good agreement with previous reports [2, 11–15] that the light gray particles were α phase and the dark gray matrix was β phase. A typical EBSD map of the rolled Mg–Li–Al–Zn alloy was shown in Fig. 1d. The Kikuchi pattern could hardly be indexed in the whole β phase region and in the deformation bands among the α phase due to the poor degree of lattice perfection. The low degree of lattice perfection in these regions can be understood to be a consequence of high dislocation density, which was induced by the rolling of the alloy plate. Since the β phase is somewhat softer than the α phase, the deformation was mainly concentrated on the β phase matrix, resulting in high dislocation density in the matrix. The grain size of the α phase are about 20–100 μm in length and 5–20 μm in width.

Figure 2 shows the microstructural information of the FSP Mg–Li–Al–Zn alloy obtained by EBSD examination. The FSP sample consisted of fine equiaxed β grains and α particles. The α particles were randomly distributed both within the β grains and at the grain boundaries (Figs. 2a–c). The average grain sizes of the α and β grains were reduced to ~1.6 and ~6.8 μm, respectively. Figure 2d, e shows the misorientation angles of all the grain boundaries and the β grain boundaries, respectively. Because the α grains were scattered on the β matrix, it is not necessary to show the misorientation angles of the α grains. The misorientation angle histograms showed that most of the grain boundaries in the FSP sample were characterized by high misorientations.

Stability of the grains in static annealing

Figure 3 shows the typical microstructures of the FSP Mg–Li–Al–Zn samples annealed for 1 h at 100, 150, 250, and 300 °C. The α phase has higher corrosion resistance than the β phase due to its lower Li content; therefore, the β matrix of the FSP samples was more severely eroded while the α particles (indicated by arrows in Fig. 3) maintained relatively smooth surfaces after the samples were etched in nitric acid solution for 2 min, as shown in Fig. 3. The SEM observations showed that the α grains exhibited a essentially uniform growth during static annealing. The average grain sizes of the α phase were ~1.8, 3.1, 6.4, and 9.2 μm for the samples annealed at 100, 150, 250, and 300 °C, respectively.

The grain boundaries of the β phase cannot be clearly observed in the etched samples which were annealed at 100 and 150 °C. The average grain size of the β phase reached 8.8 μm after the sample was annealed at 250 °C for 1 h. When annealed at 300 °C for 1 h, the β phase developed into a bimodal-sized microstructure with some large grains being surrounded by arrays of fine grains (Fig. 3d), indicating the occurrence of abnormal grain growth (AGG).

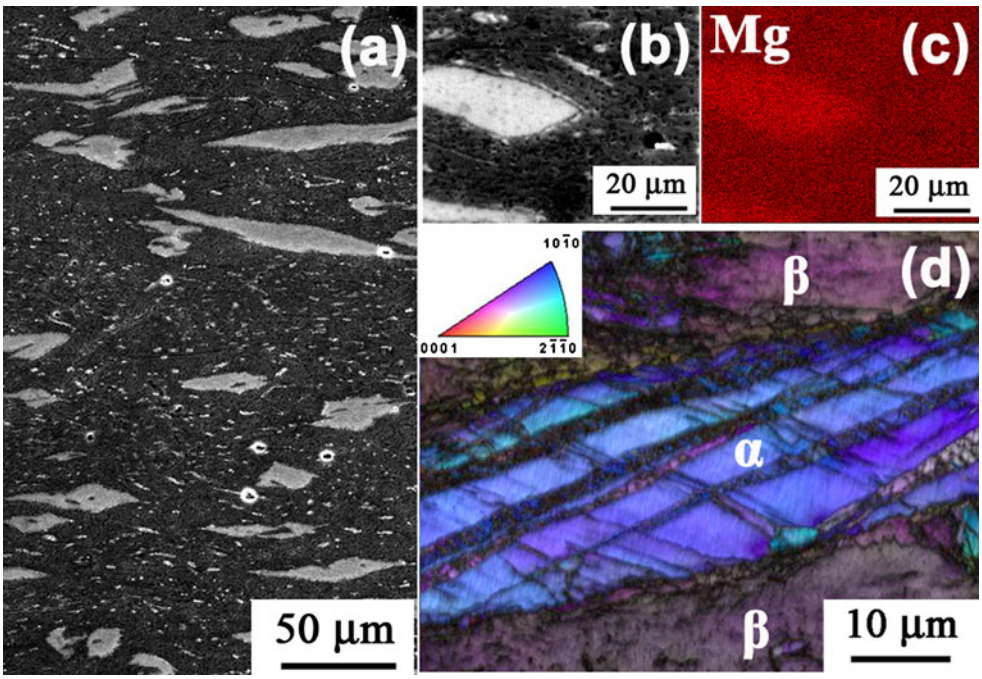

Fig. 1 Micrographs of cold rolled Mg–Li–Al–Zn alloy: **a** second electron image showing the distribution of the second phase, **b** and **c** enlarged view of a second phase and the corresponding element map of Mg, and **d** EBSD map

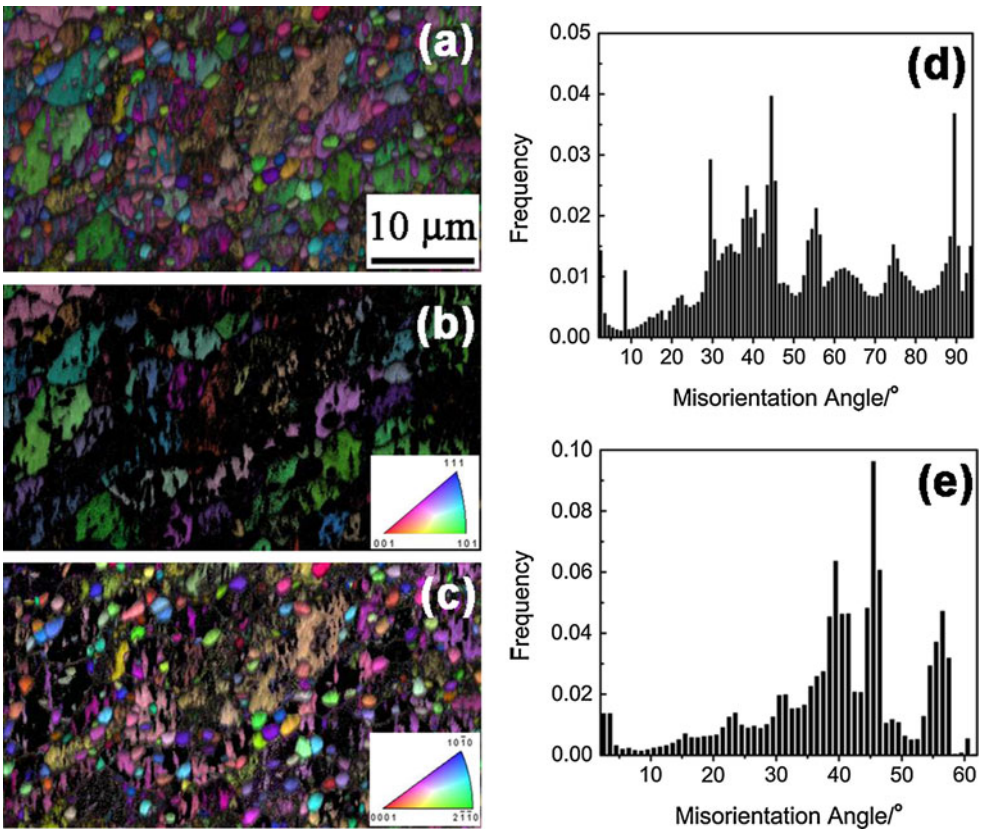

Fig. 2 Microstructure of FSP Mg–Li–Al–Zn alloy: EBSD map of **a** both of α and β grains, **b** β grains, and **c** α grains; grain boundary misorientation distribution of **d** all grain boundaries and **e** β grain boundaries

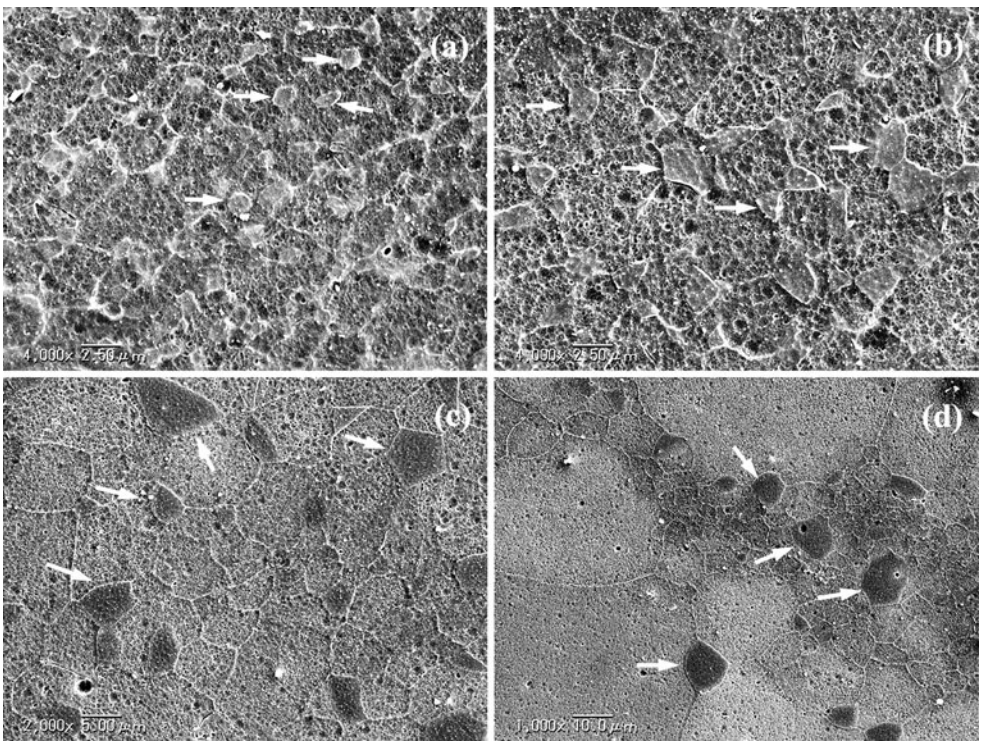

Fig. 3 SEM Microstructures of FSP Mg–Li–Al–Zn alloy annealed for 1 h at **a** 100 °C, **b** 150 °C, **c** 250 °C, and **d** 300 °C (typical α grains were indicated by *arrows*)

Superplastic behavior

Figure 4a shows the variation of elongation-to-failure as a function of the initial strain rate at various temperatures. Superplasticity was achieved over a wide temperature range of 100–300 °C. At 100 °C (i.e., 373 K, which is 0.43 T_m, where T_m is the absolute melting temperature of the Mg–Li–Al–Zn alloy), a ductility of 330 % was observed at a low strain rate of 1×10^{-5} s^{-1}. Both the elongation-to-failure and the optimum strain rate tended to increase as the temperature increased from 100 to 250 °C. A further increase in the temperature to 300 °C shifted the optimum strain rate to a higher strain rate range due to the enhanced atom diffusion rate, but reduced the ductility because of the high grain growth rate [8, 18]. Hence, a maximum superplasticity of 630 % was achieved at 1×10^{-3} s^{-1} and 200 °C in the FSP Mg–Li–Al–Zn alloy.

Figure 4b shows the effect of temperature on the ductility of the FSP Mg–Li–Al–Zn alloy at an initial strain rate of 1×10^{-2} s^{-1}. Ductility increased with an increase in the testing temperatures until it reached the maximum value of 490 % at 275 °C, and then decreased with a further increase in temperature. Though AGG occurred in the β grains when the FSP sample was annealed at 300 °C for 1 h, an elongation-to-failure higher than 400 % was achieved at a high strain rate when the tensile sample was pulled at 300 °C. This may be associated with the shorter holding time (20 min) before conducting tensile test.

Figure 5 shows the failed tensile specimens deformed at different strain rates for various testing temperatures. All the specimens show relatively uniform elongation which is the external characteristic of superplastic flow [7, 24].

Figure 6 shows the variation of flow stress (at the true strain of 0.1) with the initial strain rate for the FSP Mg–Li–Al–Zn alloy. Superplastic materials usually exhibited typical S type stress–strain rate behavior. With increasing strain rate, the strain rate sensitivity ratio m increased from low values of lower than 0.3 in Region I to a value of ~0.5 in Region II (which is the recognized superplastic deformation region) and then decreased to values of lower than 0.3 in Region III. In this study, Region III with m values of

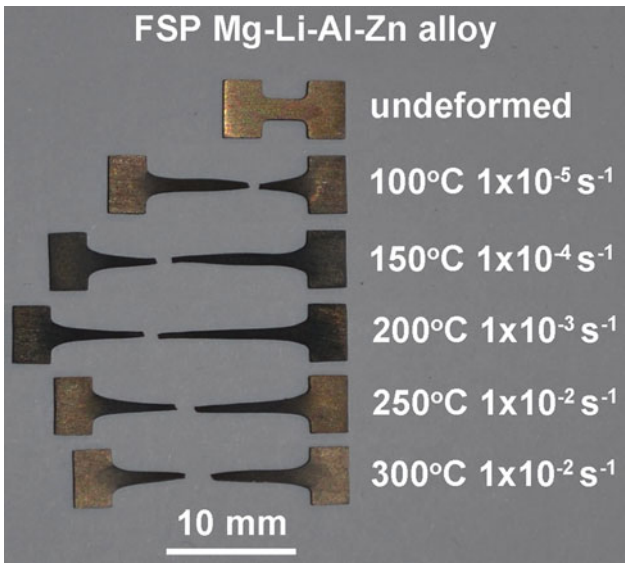

Fig. 5 Appearance of tensile specimens deformed to failure at various strain rates and temperatures for FSP Mg–Li–Al–Zn alloy

lower than ~0.3 were observed at various temperatures when the strain rate was relatively higher, indicating the disappearance of superplasticity. The m values of the FSP samples were ~0.4–0.6 in Region II, indicating that GBS is the most possible dominant deformation mechanism [5, 9, 10]. Tensile testing was not further conducted at lower strain rate when the optimum strain rate for superplasticity has been determined, because superplasticity is generally preferred to be achieved at the highest possible strain rate. For this reason, Region I was not observed in this study.

Discussions

Influence of microstructural evolution on superplasticity

The authors' pervious works have shown that FSP with water flow quenching produced ultrafine grains in Al–Zn–Mg–Cu [22] and Al–Mg–Sc alloys [17, 18], and these alloys exhibited excellent LTSP. Hofmann et al. [25]

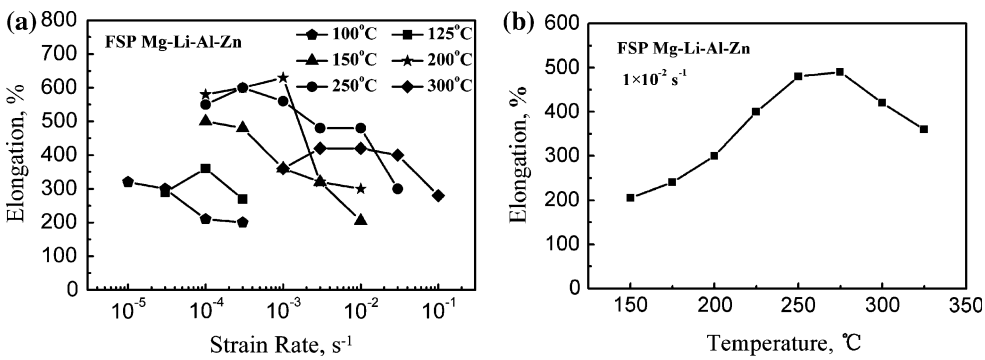

Fig. 4 Variation in elongation with **a** initial strain rate at various temperatures and **b** temperature at an initial strain rate of 1×10^{-2} s^{-1} for FSP Mg–Li–Al–Zn alloy

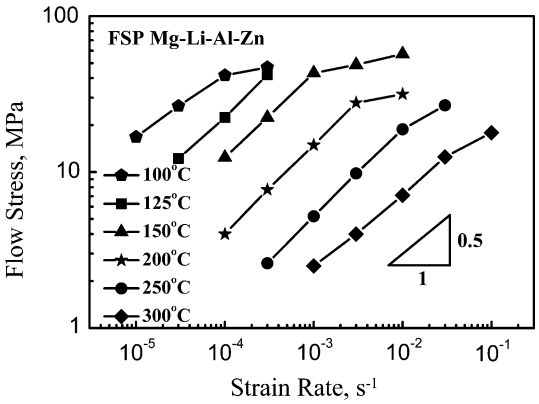

Fig. 6 Variation in flow stress with initial strain rate at various temperatures for FSP Mg–Li–Al–Zn alloy

demonstrated that submerged FSP was a method of creating ultrafine grains in 6061Al. Recently, Chai et al. [26] showed that the grain size of AZ91 Mg alloys was refined to 1.2 μm through submerged FSP while normal FSP only reduced the grain size of the AZ91 to 7.8 μm. In comparison with these reports, a combination of submerged FSP and water flow quenching would be beneficial to further reducing the FSP temperature and increasing the cooling rate, and thereby substantially retarding the grain growth during FSP. The average grain size of the α and β grains was refined to ~1.6 and ~6.8 μm, respectively, after FSP. This indicated that the combination of submerged FSP and water flow quenching is an effective method of preparing fine-grained structures in the Mg–Li–Al–Zn alloy and the grain structure of the Mg–Li–Al–Zn alloy is difficult to be refined to a submicron-scale compared to the Al alloys [17, 18, 22].

The fine-grained structure in the FSP Mg–Li–Al–Zn alloy was significantly different from that obtained by other severe plastic deformation methods. During hot rolling, the continuous β phase in the as-received Mg–Li alloy was broken into fine and equiaxed grains, and the large-sized α phase was flattened into plate-like shape by the rolling pressure and a few fine grains were developed in the α phase [27]. For the extruded Mg–Li alloys, both the α and β phase formed band-like structures with fine and equiaxed grains present within each α or β elongated band [12, 28]. Even in the Mg–Li alloys processed by the ECAP, some α grains remained clustered together [12, 13]. In the FSP Mg–Li–Al–Zn alloy, the fine α particles were randomly distributed both within the β grains and at the grain boundaries. Such a microstructure is especially suitable for superplasticity, as discussed below.

Firstly, most of the fine α grains were located at the β grain boundaries, as shown in Figs. 2 and 3. These α grains played a critical role in providing thermal stability for the β grains and thus the FSP Mg–Li–Al–Zn alloy remained fine-grained structure during superplastic deformation. Secondly, in the FSP Mg–Li–Al–Zn alloy, the tiny α grains had little contact with each other because the α grains were dispersed in the β matrix. The accommodation process of GBS would usually be the rate-controlling mechanism [29], Quantitative models have demonstrated that GBS are accommodated by either diffusion or dislocation motion [30]. The HCP α Mg has a higher melting temperature than the BCC β Li [3]. Therefore, the diffusion or dislocation motion among the α grains is sluggish compared with those among the β grains or between the α/β grains at high temperatures. In the FSP Mg–Li–Al–Zn alloy, GBS can proceed mainly along the α/β or β/β boundaries and avoid proceeding along the α/α boundaries. Therefore, compared with that obtained by other severe plastic deformation methods, in which most of α grains remained clustered together, GBS can proceed at lower temperatures or higher strain rate in the FSP Mg–Li–Al–Zn alloy due to its better accommodation process [12, 13]. Thirdly, the existence of a high fraction of HAGBs in the FSP sample was helpful to GBS during superplastic deformation. For these reasons, the FSP Mg–Li–Al–Zn alloy exhibited excellent LTSP and HSRS.

The most attractive result in this investigation is that a single-pass FSP induced (1) the appearance of LTSP at 100 °C, which is the lowest superplastic deformation temperature in the Mg–Li-based alloys, and (2) the occurrence of HSRS with elongation-to-failure of ≥400 % at temperatures of 225–300 °C, which are considered as very low temperatures for superplasticity in the Mg alloys.

Deformation mechanism

To identify the superplastic deformation mechanism, the microstructural evolution of the sample deformed at 1×10^{-3} s^{-1} and 200 °C was examined. Both the grip region that experienced static annealing and gage region that experienced dynamic annealing during superplastic deformation were investigated. Static annealing at 200 °C for about 125 min (in the grip region) led to a growth of the α and β grains from 1.6 and 6.8 to 3.6 and 8.2 μm, respectively (Fig. 7a). In the gage region, superplastic deformation led to enhanced grain growth (Fig. 7b). The grain size grew to 6.2 and 12 μm for the α and β grains, respectively. All the grains retained approximately an equiaxed shape after superplastic deformation, indicating that there is a high contribution of GBS and low contribution of dislocation glide to the total elongation [22, 31].

Some level of cavitation was also observed in the superplastically deformed gage region (Fig. 7b). During superplastic deformation, the grains slid along the grain boundaries, resulting in stress concentration at the grain boundary triple junctions. The stress concentration should be relieved by accommodation processes so that further sliding could occur, and the formation of cavitation could

be prevented. If the accommodation was not sufficient, cavities would develop. In this investigation, the cavities tended to nucleate and grow at the grain boundaries adjacent to the α phase (Fig 7b), indicating that the α grains lacked accommodative ability to successfully release the stress concentration during GBS. The growth, coalescence, and linkage of cavities limited the superplastic ductility of the FSP Mg–Li–Al–Zn alloy.

Besides the microstructural observation after superplastic deformation and the identification of m values, the activation energy, which depends on a rate-controlling process, is also an important factor in the determination of the deformation mechanism. The activation energies are shown in Fig. 8, based on

$$Q = nR\frac{\partial(\ln\sigma)}{\partial(1/T)}|\dot{\varepsilon} \quad (1)$$

where Q is the activation energy, n is the stress exponent ($n = 1/m$), R is the gas constant, σ is the applied stress, T is the absolute temperature, and $\dot{\varepsilon}$ is the strain rate. The activation energy under the constant strain rates was determined to be ~70–79 kJ/mol.

It has been reported that the lattice diffusion activation energy Q_L of the α phase and β phase are 135 and 103 kJ/mol, and the grain boundary diffusion activation energy Q_{GB} of the α phase and β phase are 92 and 67 kJ/mol [1, 32]. The activation energy of the FSP Mg–Li–Al–Zn alloy is close to but a littlie higher than the grain boundary diffusion activation energy of the β phase $Q_{GB}(\beta)$.

Figure 7 shows that both the α and β grains have been involved in the GBS during superplastic deformation. In this case, the activation energy for grain boundary diffusion between α and β grains should also be considered in addition to the activation energy for the β grain boundary diffusion. Therefore, the calculated activation energy of the FSP Mg–Li–Al–Zn alloy is a littlie higher than the $Q_{GB}(\beta)$. Because the volume of α phase is much less than that of β phase (Figs. 3, 7), the activation energy of the FSP Mg–Li–Al–Zn alloy is very close to $Q_{GB}(\beta)$, demonstrating that the GBS is mainly controlled by the grain boundary diffusion of the β phase.

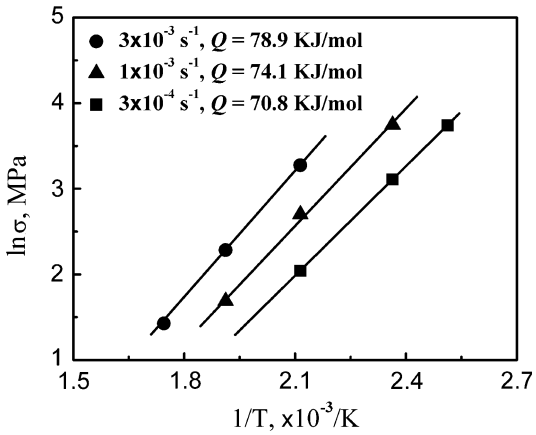

Fig. 8 Variation of ln σ as a function of reciprocal temperature for FSP Mg–Li–Al–Zn alloy

In the previous studies, the activation energy of extruded Mg–8Li–2Zn, Mg–8.5Li–1Zn, Mg–8.5Li–3Zn alloys was determined to be 90, 86, and 79 kJ mol^{-1}, respectively [14, 28], which are close to that for grain boundary diffusion in the α phase $Q_{GB}(\alpha)$. The attainment of lower activation energies close to $Q_{GB}(\beta)$ in this study can be attributed to the following factors. Firstly, a higher content of Li element (9.93 %) ensured the existence of high volume fraction of β phase in the FSP Mg–Li–Al–Zn alloy. Secondly, the fine and stable grain structures suited the occurrence of GBS among the β grains during superplastic deformation. Previous studies showed that the activation energy for creep at 150–250 °C in a Mg–9Li alloy with intermediate grain size (d = 6–35 μm) was estimated to be about 103 kJ mol^{-1} [33], which is in good agreement with the value of $Q_L(\beta)$; while the activation energy for creep at 70–150 °C in a fine-grained Mg–9Li alloy (d = 1.5–2.7 μm) was about 65 kJ mol^{-1} [8], which is close to the value of $Q_{GB}(\beta)$.

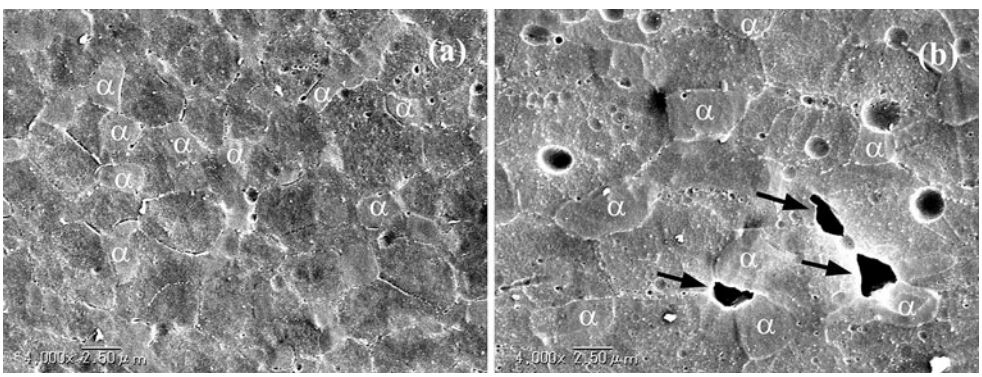

Fig. 7 SEM micrographs showing grain structures of FSP Mg–Li–Al–Zn alloy deformed to failure at 1 × 10^{-3} s^{-1} and 200 °C: **a** grip region and **b** gage region (typical α grains were labeled and cavities were indicated by *arrows*)

Conclusions

The combination of submerged FSP and water flow quenching successfully produced a mixed microstructure with fine, equiaxed, and recrystallized α and β grains surrounded by HAGBs in the Mg–Li–Al–Zn alloy. The average grain sizes of the α and β grains were ~1.6 and ~6.8 μm, respectively.

The fine α grains in the FSP Mg–Li–Al–Zn alloy played a critical role in providing thermal stability for the β grains and thus the FSP Mg–Li–Al–Zn alloy remained fine-grained structure during superplastic deformation.

The FSP Mg–Li–Al–Zn alloy exhibited a LTSP with a ductility of 330 % at 100 °C (0.43 T_m) and HSRS with elongation-to-failure of higher than 400 % at temperatures of 225–300 °C.

Microstructural examination and superplastic data analysis revealed that the dominant deformation mechanism for the FSP Mg–Li–Al–Zn alloy is GBS, which is controlled by the grain boundary diffusion of the β phase.

Acknowledgements This work was supported by the A-Star SERC (Singapore) under Grant No. 092 137 0018, and the National Natural Science Foundation of China under Grant No. 50871111.

References

1. Cao FR, Ding H, Li YL, Zhou G, Cui JZ (2010) Mater Sci Eng, A 527:2335
2. Chang TC, Wang JY, Chu CL, Lee SY (2006) Mater Lett 60:3272
3. Nayeb Hashemi AA, Clark JB, Pelton AD (1984) Bull Alloy Phase Diagr 5:365
4. Sherby OD, Wadsworth J (1989) Prog Mater Sci 33:169
5. Ma ZY, Liu FC, Mishra RS (2010) Acta Mater 58:4693
6. Langdon TG (2009) J Mater Sci 44:5998. doi:10.1007/s10853-009-3780-5
7. Liu FC, Ma ZY (2009) J Mater Sci 44:2647. doi:10.1007/s10853-009-3346-6
8. Watanabe H, Mukai T, Nieh TG, Hihashi K (2000) Scripta Mater 42:249
9. Nieh TG, Hsiung LM, Wadsworth J, Kaibyshev R (1998) Acta Mater 46:2789
10. Mishra RS, Bieler TR, Mukherjee AK (1997) Acta Metall Mater 45:561
11. Taleff EM, Ruano OA, Wolfenstine J, Sherby OD (1992) J Mater Res 7:2131
12. Yoshida Y, Cisar L, Kamado S, Kojima Y (2002) Mater Trans 43:2419
13. Wang JY, Chang TC, Chang LZ, Lee S (2006) Mater Trans 47:971
14. Dong SL, Imai T, Lim SW, Kanetake N, Saito N (2008) Mater Manuf Processes 23:336
15. Liu XH, Du GJ, Wu RZ, Niu ZY, Zhang ML (2011) J Alloys Compd 509:9558
16. Mishra RS, Ma ZY (2005) Mater Sci Eng, R 50:1
17. Liu FC, Ma ZY, Chen LQ (2009) Scripta Mater 60:968
18. Liu FC, Ma ZY (2010) Scripta Mater 62:125
19. Liu FC, Ma ZY (2011) Mater Sci Eng, A 530:548
20. Liu FC, Xue P, Ma ZY (2012) Mater Sci Eng, A 547:55
21. Johanes LB, Mishra RS (2007) Mater Sci Eng, A 464:255
22. Ma ZY, Mishra RS, Liu FC (2009) Mater Sci Eng, A 505:70
23. Yang Q, Xiao BL, Ma ZY, Chen RS (2011) Scripta Mater 65:335
24. Shin HS, Jeong YJ, Ahn JH (2007) J Alloys Compd 434–435:40
25. Hofman DC, Vecchio KS (2005) Mater Sci Eng, A 402:234
26. Chai F, Zhang DT, Li YY, Zhang WW (2013) Mater Sci Eng, A 568:40
27. Dong HW, Xu SW, Wang LD, Kamado S, Wang LM (2012) Metall Mater Trans A 13:709
28. Liu XH, Zhang HB, Gu SH, Qu ZK, Wu RZ, Zhang ML (2011) Mater Sci Eng, A 528:6157
29. Jiménez-Melendo M, Domínguez-Rodríguez A, Holgado-Salado M (2001) Int J Plast 17:341
30. Edington JW, Melton KN, Cutler CP (1976) Prog Mater Sci 21:63
31. Liu FC, Ma ZY (2008) Scripta Mater 59:882
32. Frost HJ, Ashby MF Deformation-mechanism maps, the plasticity and creep of metals and ceramics. http://Thayer.dartmouth.edu/defmech
33. Metenine P, Gonzalez-Doncel G, Ruano OA, Wolfenstine J, Sherby OD (1990) Mater Sci Eng, A 125:195